Optimizing Bend-Loss in Optical Waveguide Channel Routing on Photonic Integrated Circuits

Sumit Sharma
IIT Roorkee: Indian Institute of Technology Roorkee
Sudip Roy (sudip.roy@cs.iitr.ac.in)
Indian Institute of Technology Roorkee https://orcid.org/0000-0001-7873-3069

Research Article

Keywords: Channel routing, detailed routing, design automation, optical circuits

Posted Date: May 26th, 2022

DOI: https://doi.org/10.21203/rs.3.rs-1652266/v1

Optimizing Bend-Loss in Optical Waveguide Channel Routing on Photonic Integrated Circuits

Sumit Sharma and Sudip Roy

CoDA Laboratory, Department of Computer Science and Engineering
Indian Institute of Technology (IIT) Roorkee, India.

Contributing authors: ssharma6@cs.iitr.ac.in; sudip.roy@cs.iitr.ac.in;

Abstract

Silicon photonics (Si-photonics) has been established as a potential technology that integrates both electronic and optical circuits on single integrated circuits (ICs) in order to satisfy the increasing demand for high-speed and low-power in the emerging market of ICs. It has opened up the research directions in the domain of design automation for photonic ICs. On the physical layout of the optical circuits, it is a challenging task to obtain the optimal routing of optical waveguides, while minimizing all the parameters like the number of tracks, total bend loss, worst signal loss, total propagation loss and total crossing loss. In this paper, we proposed two non-Manhattan grid-based methods for reducing the bend loss, worst signal loss and tracks in optical channel routing. First, a 0-1 integer linear programming (ILP) based algorithm called *minimizing bend loss* (*MBL*) is proposed, which minimizes the total bend loss (*TBL*) and the worst signal loss (*WSL*) while reducing the number of tracks ($\boldsymbol{T}$) over the state-of-the-art technique. The execution time of *MBL* is very high for the large input. Hence next, a scalable heuristic called *reducing bend loss* (*RBL*) is presented that provides a better balance between the reduction of the *TBL* and $\boldsymbol{T}$ over the state-of-the-art and *MBL* algorithms. Simulation results show that *MBL* can reduce the *TBL* and the *WSL* by an average of 57.9% and 63.1%, respectively, with an average increase of 12% in $\boldsymbol{T}$ over state-of-the-art algorithms. The simulation results show that the *RBL* reduces the *TBL* and the *WSL* by an average of 39.7% and 41.3%, respectively, with an average increase of 23.7% in $\boldsymbol{T}$ over state-of-the-art algorithms.

Keywords: Channel routing, detailed routing, design automation, optical circuits

1 Introduction

Due to the continuous increase in transistor count and increasing demand for high-speed and low-power consumption in the integrated circuits, Moore's law [1] is reaching its limit. Moreover, the need for high-performance and low-power circuits requires other non-transistor alternatives to the traditional very-large-scale integration (VLSI) industry. Hence, researchers are investigating several alternative technologies, such as reversible computing, quantum computing, silicon photonics and quantum photonics [2]. Among all, silicon photonics (Si-photonics), which is the integration of photonics and electronics on a single integrated circuit (IC) chip, is one of the potential technologies for next-generation computing [3]. This technology is rapidly growing as a platform for large-scale photonic integrated circuits (PICs) due

to low fabrication cost, smaller footprint, low-power consumption, and CMOS compatibility to basic CMOS electronics [1]. The advancement in PICs has opened a wide variety of applications in the field of telecommunications, photonic signaling, data center, high-performance computations, spectroscopy, optical network-on-chip (ONoC), chip designing, medical diagnostics, and biosensing [2].

ONoC is one of the promising applications, where in place of metal wires optical interconnects/waveguides are used to satisfy the need for high bandwidth with lesser power dissipation. Current ONoC architectures can be classified into two categories: wavelength-routed and control-networks-based [4]. The layout of these optical networks is determined with the topology- mesh, torus, ring and mixed [5]. However, the design of topologies should limit the number of laser sources and the optical links, as laser source coupling is one of the main contributors to the chip packaging costs. Further, as the number of photonic elements and the size of optical interconnects increase on the optical network, the need for physical layout optimization (placement and routing) arises. However, for the complete adoption of large-scale photonic networks and interconnects, the design and fabrication of optical components first need to address the operational (optical power, on-chip temperature variations) and fabrication (optical waveguide properties, signal losses, area) challenges [5].

For the past few years, researchers have focused on the placement and global routing [6–9] of the on-chip optical components and interconnect. In many optical networks [10, 11], the column-based placement of the photonic elements is performed to minimize signal loss and area. This column-based arrangement of components makes the vertical routing region (channels) between the devices, leading to the channel routing problem. To date, several researchers have presented techniques for channel routing in PICs for minimizing the signal loss and area [12–14]. While obtaining the channel routing of optical waveguides, the bend geometry has a vital role in reducing the bend loss. The sharper bends having the smaller bend angles have more impact on the signal loss. Therefore, the minimization of bend loss is a primary objective in optical waveguide routing. This work focuses on the removal of bendings having higher losses. The contributions of this paper are summarized as follows.

1. A 0-1 integer linear programming (ILP) is formulated for minimizing the bend loss (*MBL*) while reducing the number of tracks in optical channel routing.
2. A new grid-based restricted routing is proposed to eliminate the sharper bends having smaller bend angles.
3. A heuristic is proposed for reducing the bend loss (*RBL*) in the optical channel routing.
4. A comparative analysis of the simulated test-cases shows that the proposed ILP formulation outperforms the state-of-the-art techniques in terms of the total bend loss, the worst signal loss, and the number of tracks.

The rest of the paper is organized as follows. Sec. 2 discusses the basic concepts and the prior works in optical channel routing. The motivation and problem formulation are discussed under Sec. 3, respectively. A 0-1 integer linear programming (ILP) formulation of optical waveguide channel routing for minimizing the bend loss, worst signal loss while reducing the number of tracks is presented in Sec. 4. Further, the proposed heuristic for optical channel routing is presented in Sec. 5. The results and comparative study are are discussed under Sec. 6. Finally, Sec. 7 concludes this paper.

2 Basic Preliminaries and Prior Works

This section presents the basic preliminaries and the related works in the domain of optical channel routing.

2.1 Basic Preliminaries

This section provides a brief overview of the basics of optical channel routing. Table 1 represents all the symbols used in this work.

2.1.1 Channel Grid

The channel routing of optical waveguides in the proposed work follows a grid-based non-Manhattan routing. Channel is represented as a space between the list of optical pins that are present on its two opposite sides. Fig. 1 depicts the

Table 1: List of used symbols.

Symbol	Description
H	Height of the channel
W	Width of the channel
h	Grid cell height
w	Grid cell width
N	Number of optical waveguides
T	Number of tracks
$angles$	Set of all possible types of bend angles
α	An angle with 90° bend
θ	An angle with θ° bend
ϕ	An angle with ϕ° bend
$bend(x)$	An x-angled bend
$Nbends(x)$	Total number of bends with x-angle
BL	Bend loss
$BL(x)$	Bend loss at x angled bend
TBL	Total bend loss
TPL	Total propagation loss
TCL	Total crossing loss
TSL	Total signal loss
WSL	Worst signal loss
TWL	Total waveguide length
$r_{i,j}$	A Boolean variable for a grid point at a location of i^{th} track and j^{th} column from bottom and left side of the channel, respectively
$c_{i,j}$	A Boolean variable for the crossing of waveguides at a grid location of i^{th} track and j^{th} column from bottom and left of the channel, respectively
Ein_{o,i_1,j_1,i_2,j_2}	A Boolean variable for a channel grid point (i_1, j_1) with an incoming optical waveguide o routing from a location of (i_2, j_2)
$Eout_{o,i_1,j_1,i_2,j_2}$	A Boolean variable for a channel grid point (i_1, j_1) with an outgoing optical waveguide o routing to a location of (i_2, j_2)

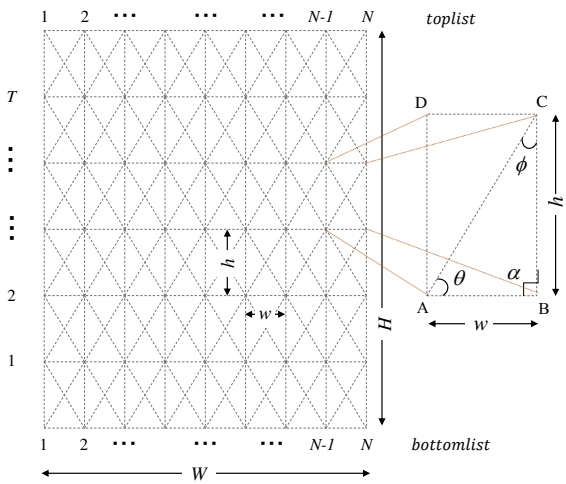

Fig. 1: A channel routing grid and cell.

grid structure used in our work, where *toplist* and *bottomlist* are two lists of optical terminals along a rectangular channel whose width and height are represented as W and H, respectively. The terminals of both lists are assigned with a number p $(1 \leq p \leq N)$. The terminals with the same number are connected with an optical interconnect p during routing. To implement a channel routing, the channel is divided into a grid of uniform cells

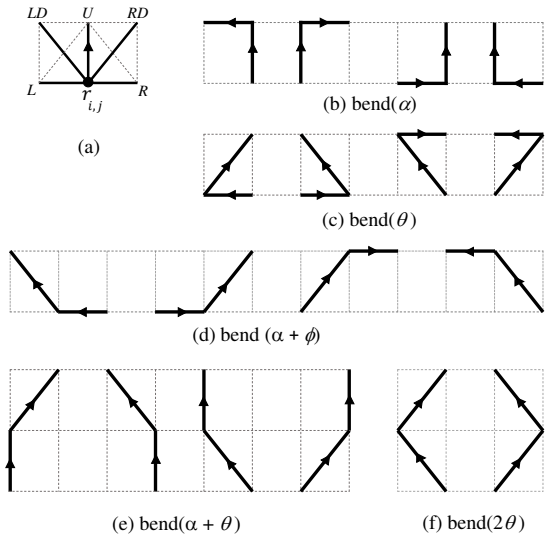

Fig. 2: (a) Possible routing directions from any grid point $(r_{i,j})$, and (b–f) types of bends in the channel routing.

with the width and height of w and h, respectively. Each row in the grid contains different permutations of terminal numbers that decide the path of optical interconnects within a channel. These rows are called tracks. Hence, the number of tracks (T) decides the size/area of the channel.

2.1.2 Routing Paths and Bends

As mentioned above, our work is based on the non-Manhattan grid routing, where an optical waveguide always routes from bottom to top boundary terminals. Hence, from any point inside the channel grid, a waveguide can possibly move in five directions, i.e., left (L), right (R), left-diagonal (LD), right-diagonal (RD), and vertical up (U), as shown in Fig. 2 (a). On a track, when an optical waveguide changes its direction from the previous track direction, then it results in a bend in its path. The closed view of a grid cell in Fig. 1 shows that the cell diagonal results two different angles of $\theta = tan^{-1}(\frac{h}{w})$ and $\phi = (90 - \theta)$ with its boundary. Hence, the movement of an optical waveguide in the channel grid results in five different types of bends with an angle of α, θ, $\alpha + \phi$, $\alpha + \theta$, and 2θ, where α represents a 90° angle. Figs. 2(b)-(f) show all the possible types of routing bends that can occur while routing from bottom to top directions.

2.1.3 Types of Losses

Based on the exploration of different routing geometries following three types of losses (with dB unit), bending loss, crossing loss, and length loss can be treated as the penalty in optical planar routing.

i) Bend Loss: For a given optical bend with two unit-length waveguides, bend radius (R), and a bend angle (ψ). The bend loss (BL) can be computed with Equation (1) [13].

$$BL(\psi) = 0.0041 \cdot \psi \cdot R^{-1.6} \tag{1}$$

which indicates the bend loss $BL(\psi)$ is directly proportional to the bend angle and inversely proportional to the bend radius.

ii) Popagation Loss: The propagation loss (PL_i) of a given optical waveguide i is proportional to the length (ℓ_i) and is defined as $PL_i = 3 \cdot 10^{-9} \cdot \ell_i$. From the viewpoint of optical signal loss, propagation/length loss on an optical waveguide is very small [13].

iii) Crossing Loss: When two optical waveguide cross each other, it results in some signal loss, which is named as crossing loss. According to the prior experimental work, it has been detected that the crossing loss of two optical nets is constant, i.e., in the range of (0.1–0.2 dB) per crossing.

2.1.4 Total Signal Loss (TSL)

TSL is the sum of the total bend loss (TBL), the total propagation loss (TPL) and the total crossing loss (TCL).

2.1.5 Worst Signal Loss (WSL)

The routing of each optical waveguide reduces the optical signal strength along its path due to the above-mentioned losses. For an N number of different routed paths, the worst signal loss (WSL) is defined as the maximum signal loss among these paths.

$$WSL = \max_{j=1}^{N} \ell oss_j \tag{2}$$

where ℓoss_j is the optical loss for an optical waveguide j along its routed path.

2.2 Prior Works

In the routing of optical interconnects with the photonic integrated devices, researchers have explored many techniques while satisfying the optical properties and the design constraint rules like the minimum distance between waveguides, waveguide width, and area, etc. [13, 14]. Since the complete routing can be realized by performing the detailed/channel routing after global routing. Hence, in the past channel routing has been performed on PICs for minimizing the total signal loss (TSL) and area [13, 14], where the area is regarded as the function of the total length of waveguides and the number of tracks used in channel routing.

Condart *et al.* [15] presented the first work on optical channel routing, which was the adaptation of basic VLSI placement and routing in the optical domain. The optical routing is performed on Manhattan grid-based channels without considering optical waveguide geometries and crossing properties, resulting in a higher signal loss due to sharp bends. In [12] and [13] a *2SWAP* channel routing based on the traditional *SWAP* [16] algorithm is proposed that shows the reduction in the total number of crossing and bends. *2SWAP* reduces the 90° bends by using the additional bends of 135°. Hence, *2SWAP* [13] reduces the signal loss than [15] with an overhead of increased number of tracks, i.e., area. Another non-Manhattan-based channel routing is introduced in [13], which used the basic left edge algorithm with the knock-knee method. This method shows the track reduction at the cost of higher bend loss compared to *2SWAP*. Moreover, [13] follows a restricted constraint of 90° crossing between two crossed waveguides, which is not mandatory for on-chip optical interconnects. A more flexible channel routing (TNR) has been presented in [14] that removed 90° crossing constraints while maintaining a crossing angle in the range of 60°–120°. A new rectangular grid-based non-Manhattan routing model in TNR showed the reduction in bend loss by replacing the sharpen bends with smooth bends. In TNR, both the tracks and bends are reduced by using the existing modified two-pass optimality-oriented hierarchical bubble sorting algorithm [17]. However, still the presence of 90° bends in TNR results the higher bend loss. Moreover, this new routing within the rectangular grid model may violate the

design rule check of minimum spacing distance among the waveguides.

3 Motivation and Problem Formulation

In this section, we discuss the motivation and problem statement of our work.

3.1 Motivation

The main objective of any routing problem is to route all the waveguides while reducing the *TSL* and area, i.e., tracks (T). In the routing of optical waveguides, bend loss and number of crossing are the two significant figures of merits in designing high-density PICs [18, 19]. The higher radiation loss at the sharp bends limits the density of a PIC. Different approaches have been proposed in the literature to reduce *TBL*, where the curvilinear nature of optical waveguides plays an essential role [19]. Due to the curvilinear shapes, the performance of the optical circuit depends on the number of bends, bend radius, and width of the waveguides [20]. As discussed above, the routing grid in [14] considers the optical waveguide geometries and shows the reduction in bend loss compared to the prior work. In this work, we have used the channel grid structure similar to the [14]. However, to further reduce the bend loss, a restricted horizontal routing is used to eliminate the α and θ bends. Further, the lack of multi-layer routing results in the crossing between waveguides, which can be reduced by controlled crossings. Moreover, each crossing has a constant loss. Therefore, bend loss minimization is of pivotal importance to design high-density PICs. Further, there is an overhead between *TBL* and T reduction. In this work, we are balancing these parameters with an ILP formulation to minimize the bend loss while reducing the area and *WSL*.

3.2 Problem Formulation

This work aims to provide a routing path to the optical waveguides within a rectangular region/channel, where the two opposite sides, i.e., bottom and top boundaries of the channel have fixed terminal pins. Each pin that corresponds to the same waveguide must be connected from bottom to top while satisfying the routing constraints. The channel is assumed to be a grid (Fig. 1), where each net can route in five directions from the current grid point, as shown in Fig. 2.

Input: Given the bottom list and the top list of N number of optical waveguides.

Output: The routing path for each given optical waveguide from bottom list to the top list within the channel.

Objective: The main objectives of this channel routing are: (i) to minimize the total bend loss (*TBL*), (ii) to minimize the worst (maximum) signal loss (*WSL*) along the optical path, and (iii) to minimize the number of tracks (T), which has been defined as a multi-objective weighted function f as:

$$\begin{aligned} & Minimize\ f \\ & f = \left(\delta * TBL + \beta * WSL + \gamma * T\right) \\ \text{s.t.} \quad & \delta + \beta + \gamma = 1 \text{ and } \delta,\ \beta,\ \gamma\ \epsilon\ \mathbb{R} \end{aligned}$$

where δ, β, and γ are user defined weighted parameters.

4 0-1 Integer Linear Programming (ILP) Formulation for Minimizing Bend Loss (*MBL*) in Optical Channel Routing

The routing of each optical waveguide reduces the optical signal strength along its path due to various losses (as mentioned in Sec. 2.1). Hence in addition to optimize the *TBL*, *WSL* should also be reduced. Further, any routing aims to reduce the area. Therefore the T should also be reduced to decrease the total channel area. In this section, a constraints-based 0-1 integer linear programming (ILP) formulation for optical channel routing has been introduced to minimize the bend loss (*MBL*). For the ILP formulation, we have considered the same $N \times T$ grid-based optical channel, as mentioned in Sec. 2.1, where N is the number of terminals and T is the number of tracks. We have formulated a 0-1 ILP model for minimizing the multi-objective function f as follows:

$$Minimize\ f = \left(\delta * TBL + \beta * WSL + \gamma * T\right)$$

$$TBL = \sum_{x}^{x\ \epsilon\ angles} Nbends(x) \cdot BL(x) \quad (3)$$

$$Nbends(x) = \sum_{i=1}^{T}\sum_{j=1}^{N} bend(x)_{i,j} \quad (4)$$

where TBL, WSL are defined as Equations (3), (2), N is the total number of optical waveguides in the given bottom list, T is the number of tracks, $i = (1, \ldots, T)$, $j = (1, \ldots, N)$, $angles = (\alpha, \theta, \alpha+\phi, \alpha+\theta, 2\theta)$ is the set of all possible types of angles in channel grid (as depicted in Fig. 2), $Nbend(x)$ is the total number of x-angle bends, $BL(x)$ is the bend loss for x-angle bend, $bends(x)_{i,j}$ indicates an x-angle bend at i^{th} track and j^{th} column in grid. In Equation (3), TBL is defined as the sum of all the bend losses along the channel grid points, where $Nbends(x)$ and $BL(x)$ can be calculated using Equations (4) to (6) and Equation (1), respectively.

1) Bending Constraints: The presence of all possible types of bends (as depicted in Fig. 2) at every grid location (i, j) can be identified with the following Equations (5) to (6).

$$\begin{aligned} bend(\alpha)_{i,j} = (&Ein_{o,i,j,i-1,j} * (Eout_{o,i,j,i,j-1} \\ &+ Eout_{o,i,j,i,j+1})) + ((Ein_{o,i,j,i,j-1} \\ &+ Ein_{o,i,j,i,j+1}) * Eout_{o,i,j,i+1,j}) \end{aligned} \quad (5)$$

$$\vdots$$

$$\begin{aligned} bend(2\theta)_{i,j} = &(Ein_{o,i,j,i-1,j+1} * Eout_{o,i,j,i+1,j+1}) \\ &+ (Ein_{o,i,j,i-1,j-1} * Eout_{o,i,j,i+1,j-1}) \end{aligned} \quad (6)$$

where Ein_{o,i_1,j_1,i_2,j_2} is a Boolean variable for a channel grid point (i_1, j_1) with an incoming optical waveguide o routing from (i_2, j_2) location, $Eout_{o,i_1,j_1,i_2,j_2}$ is a Boolean variable for a channel grid point (i_1, j_1) with an outgoing optical waveguide o routing to (i_2, j_2) location. Equation (5) calculates the presence or absence of an α bend at (i, j) grid location that would be better understood with Fig. 2(b). $Ein_{o,i,j,i-1,j}$, $Ein_{o,i,j,i,j-1}$, and $Ein_{o,i,j,i,j+1}$ are the incoming optical waveguides (o) from the previous track $(i-1)$ in vertical up (U) direction, from the same track (i) in left (L) and right (R) directions, respectively to the (i, j) location. $Eout_{o,i,j,i,j-1}$, $Eout_{o,i,j,i,j+1}$ and $Eout_{o,i,j,i+1,j}$ are the outgoing optical waveguide (o) from the (i, j) grid location routing to the same track (i) in L, R directions, and to the next track $(i+1)$ in U direction, respectively. Similarly, the remaining bends can be interpreted with Figs. 2(b)–(f), respectively.

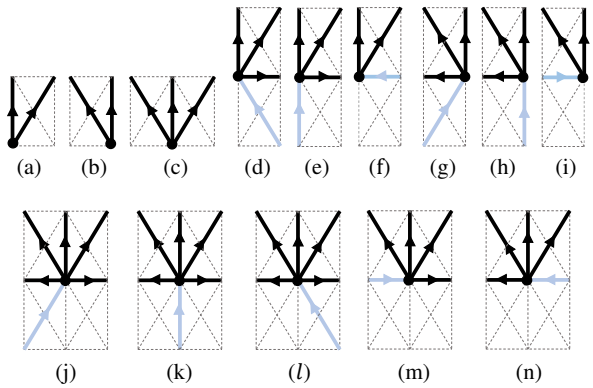

Fig. 3: Routing constraints from a grid point (black dot), where the blue and black lines indicate the incoming and outgoing waveguides, respectively (a–c) bottom boundary of the grid, (a) bottom–left, (b) bottom–right, (c) remaining bottom points, (d–n) internal grid points along the tracks (d–f) left boundary, (g–i) right boundary, and (j–n) remaining internal points.

$$\begin{aligned} \forall_{x\ \epsilon\ angles}\forall_{i,j}\ bend(x)_{i,j} = 0 \text{ or } 1, \\ i = 0, 1, \ldots, T;\ j = 1, 2, \ldots, N \end{aligned} \quad (7)$$

2) Routing Constraints: The routing of an optical waveguide from a grid location follows some restrictions to maintain the bottom-up paths for all the given waveguides. These restrictions are explained in Equations (8) to (10) and diagrammatically presented in Fig. 3.

$$r_{0,j} = \begin{cases} Eout_{o,0,j,1,j} + Eout_{o,0,j,1,j+1}, & \text{if } j = 1 \\ Eout_{o,0,j,1,j-1} + Eout_{o,0,j,1,j}, & \text{if } j = N \\ Eout_{o,0,j,1,j-1} + Eout_{o,0,j,1,j} & \\ +Eout_{o,0,j,1,j+1}, & \text{otherwise} \end{cases} \quad (8)$$

The routing constraints for the bottom boundary ($r_{0,j}$) have been illustrated in Figs. 3(a–c) and explained in Equation (8). In Figs. 3(a) and (b), the routing constraints for the bottom-left ($j = 1$) and bottom-right ($j = N$) are shown where the waveguide (o) can move to the next track in two possible directions (U or R) and (L or U), respectively. While Fig. 3(c) represents the routing constraints for the remaining bottom points ($2 \leq j \leq N$), where a waveguide can move to the next track by taking one of the possible path (L or U or R).

$$r_{i,j} = \begin{cases} \Big((Ein_{o,i,j,i-1,j} + Ein_{o,i,j,i-1,j+1}) \\ *(Eout_{o,i,j,i+1,j} + Eout_{o,i,j,i+1,j+1} \\ +Eout_{o,i,j,i,j+1})\Big) + \Big(Ein_{o,i,j,i,j+1} \\ *(Eout_{o,i,j,i+1,j} + Eout_{o,i,j,i+1,j+1})\Big), \\ \qquad\qquad \text{if } j = 1 \\ \Big((Ein_{o,i,j,i-1,j-1} + Ein_{o,i,j,i-1,j}) \\ *(Eout_{o,i,j,i,j-1} + Eout_{o,i,j,i+1,j-1} \\ +Eout_{o,i,j,i+1,j})\Big) \\ +\Big(Ein_{o,i,j,i,j-1} * (Eout_{o,i,j,i+1,j-1} \\ +Eout_{o,i,j,i+1,j})\Big), \\ \qquad\qquad \text{if } j = N \\ \Big((Ein_{o,i,j,i-1,j-1} + Ein_{o,i,j,i-1,j} \\ +Ein_{o,i,j,i-1,j+1}) * (Eout_{o,i,j,i,j_\ell} \\ +Eout_{o,i,j,i+1,j-1} + Eout_{o,i,j,i+1,j} \\ +Eout_{o,i,j,i+1,j+1} + Eout_{o,i,j,i,j+1})\Big) \\ +\Big(Ein_{o,i,j,i,j-1} * (Eout_{o,i,j,i+1,j-1} \\ +Eout_{o,i,j,i+1,j} + Eout_{o,i,j,i+1,j+1} \\ +Eout_{o,i,j,i,j+1})\Big) \\ +\Big(Ein_{o,i,j,i,j+1} * (Eout_{o,i,j,i,j-1} \\ +Eout_{o,i,j,i+1,j-1} + Eout_{o,i,j,i+1,j} \\ +Eout_{o,i,j,i+1,j+1})\Big), \\ \qquad\qquad \text{otherwise} \end{cases} \tag{9}$$

Similarly, the routing constraints for all remaining grid points along the channel tracks are shown in Figs. 3(d–n), which are formally explained with Equation (9). The routing constraints for a grid point at the left boundary (other than the bottom boundary) of the channel, i.e., $i \geq 1$ and $j = 1$, are represented with Figs. 3(d–f). As shown in Figs. 3(d–e), the incoming optical waveguides $Ein_{o,i,j,i-1,j}$ and $Ein_{o,i,j,i-1,j+1}$ that come from the previous track $(i-1)$ in either U or LD directions can route in one of the three possible output paths by either moving to the next track in U or RD directions or moving to the same track in R direction, respectively. However, the incoming waveguide $Ein_{o,i,j,i,j+1}$ can only have two output paths routing to the next track by moving in either U or RD directions, as depicted in Fig. 3(f). Similarly, the routing constraints for the right boundary points (other than the bottom boundary), i.e., $i \geq 1$ and $j = N$, are depicted in Figs. 3(g–i). Otherwise, for the remaining internal grid points, i.e., $i \geq 1$ and $2 < j < N$, the five different routing constraints are shown in Figs. 3(j–n). When an optical waveguide comes from the previous track at these internal points, it can route in any of the five different paths (Figs. 3(j–l)). However, as shown in Figs. 3(m–n), the incoming waveguide from the same track can route to four possible paths.

Equation (10) defines that from each grid point atleast one optical waveguide should pass.

$$\forall_{i,j}\ r_{i,j} = 1, \quad i = 0, 1, \ldots, T; \quad j = 1, 2, \ldots, N \tag{10}$$

Further, each outgoing waveguide from a grid location of (i_1, j_1) to (i_2, j_2) should becomes the incoming waveguide for the (i_2, j_2) location. Therefore, if $Eout_{o,i_1,j_1,i_2,j_2} = 1$, then Ein_{o,i_2,j_2,i_1,j_1} should be 1. However, when $Eout_{o_1,i,j_1,i,j_2} = 1$, i.e., an outgoing waveguide o_1 is present from (i, j_1) to (i, j_2), then to avoid the overlap of horizontal waveguides there should be no outgoing waveguide from (i, j_2) to (i, j_1), i.e., $Eout_{o_2,i,j_2,i,j_1} = 0$.

3) Crossing Constraints: Furthermore, whenever a waveguide route in the horizontal L or R direction from a grid location of (i, j_1) to (i, j_2), then it may cross with another waveguide that was already routed at (i, j_2) location. Hence, each grid point is assigned with a Boolean variable $c_{i,j}$ representing the crossing of waveguides at (i, j) grid location. The crossing constraints are defined in Equations (11) to (13) and diagrammatically presented in Fig. 4.

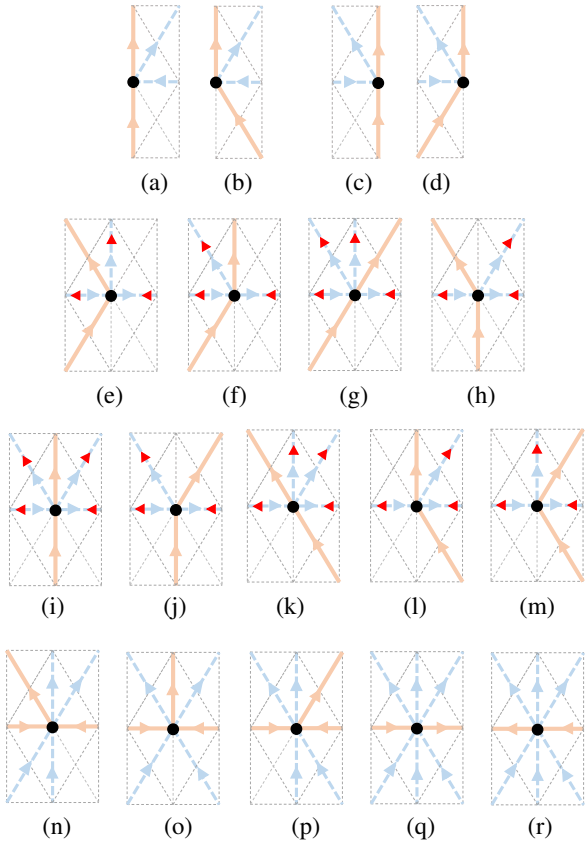

Fig. 4: All the possible cases of crossing constraints for a grid point (black dot), where orange lines indicate the previously routed waveguide, while blue dotted lines with blue and red arrows indicate the possible routing for other waveguides from black grid point (a–b) left boundary, (c–d) right boundary, and (e–r) remaining internal grid points along tracks.

$$\forall_j \; c_{0,j} = 0, \qquad j = 1, 2, \ldots, N \tag{11}$$

$$\forall_{i,j} \; c_{i,j} = 0 \text{ or } 1, \quad i = 1, 2, \ldots, T; \quad j = 1, 2, \ldots, N \tag{12}$$

The waveguides at the bottom-boundary grid points do not cross each other hence $c_{0,j} = 0$, as mentioned in Equation (11). However, for all the internal grid points with $i > 0$, there may be the crossing of two waveguides with each other hence $c_{i,j} = 0$ or 1, as mentioned in Equation (12).

$$c_{i,j} = \begin{cases} Ein_{o_2,i,j,i,j+1} * Eout_{o_2,i,j,i+1,j+1}, \\ \qquad \text{if } j = 1 \;\&\; \big(case(a) \text{ or } case(b)\big) = 1 \\ Ein_{o_2,i,j,i,j-1} * Eout_{o_2,i,j,i+1,j-1}, \\ \qquad \text{if } j = N \;\&\; \big(case(c) \text{ or } case(d)\big) = 1 \\ \Big(Ein_{o_2,i,j,i,j-1} * (Eout_{o_2,i,j,i+1,j} \\ + Eout_{o_2,i,j,i,j+1})\Big) + \Big(Ein_{o_2,i,j,i,j+1} \\ * (Eout_{o_2,i,j,i+1,j} + Eout_{o_2,i,j,i,j-1})\Big), \\ \qquad \text{if } j = (2, \ldots, N-1) \;\&\; case(e) = 1 \\ \Big(Ein_{o_2,i,j,i,j-1} * (Eout_{o_2,i,j,i+1,j-1} \\ + Eout_{o_2,i,j,i,j+1})\Big) + \Big(Ein_{o_2,i,j,i,j+1} \\ * (Eout_{o_2,i,j,i+1,j-1} + Eout_{o_2,i,j,i,j-1})\Big), \\ \qquad \text{if } j = (2, \ldots, N-1) \;\&\; case(f) = 1 \\ \Big(Ein_{o_2,i,j,i,j-1} * (Eout_{o_2,i,j,i+1,j-1} \\ + Eout_{o_2,i,j,i+1,j} + Eout_{o_2,i,j,i,j+1})\Big) \\ + \Big(Ein_{o_2,i,j,i,j+1} * (Eout_{o_2,i,j,i+1,j-1} \\ + Eout_{o_2,i,j,i+1,j} + Eout_{o_2,i,j,i,j-1})\Big), \\ \qquad \text{if } j = (2, \ldots, N-1) \;\&\; case(g) = 1 \\ \qquad \vdots \\ (Ein_{o_2,i,j,i-1,j-1} + Ein_{o_2,i,j,i-1,j}) \\ * (Eout_{o_2,i,j,i+1,j} + Eout_{o_2,i,j,i+1,j+1}), \\ \qquad \text{if } j = (2, \ldots, N-1) \;\&\; case(n) = 1 \\ \qquad \vdots \\ (Ein_{o_2,i,j,i-1,j-1} + Ein_{o_2,i,j,i-1,j} \\ + Ein_{o_2,i,j,i-1,j+1}) * (Eout_{o_2,i,j,i+1,j-1} \\ + Eout_{o_2,i,j,i+1,j} + Eout_{o_2,i,j,i+1,j+1}), \\ \qquad \text{if } j = (2, \ldots, N-1) \;\& \\ \qquad \big(case(q) \text{ or } case(r)\big) = 1 \end{cases} \tag{13}$$

If a waveguide (o_1) is already present at (i, j) location, then the routing of another waveguide (o_2) has some restrictions as depicted in Fig. 4, where the orange lines indicate the o_1 (already routed) and blue dotted lines refer to o_2 (to be routed). These constraints are explained in Equation (13), where $case(a)$, $case(b)$, ... , $case(r)$ correspond to the presence of previous routed waveguide

Algorithm 1 *MBL*

Input: *bottomlist*, *toplist*, N, T_{max}, T_{min}
Output: Routing results (T, *TBL*, *WSL*, and *TWL*) of the optical channel grid

1 **for** *each t in the range of [1, N]* **do**
2 Generate the ILP model for a grid size of $N \times t$ with Equations (5) to (13); Perform and store the routing result for the ILP model while minimizing the *TBL* and *WSL*;
3 **end**
4 Find the best solution from these t routings with the minimum loss and reduced tracks;
5 **return** *Routing results having the minimized parameters;*

as shown Fig. 4(a), Fig. 4(b), ... , Fig. 4(r), respectively.

Along the left-boundary, if a waveguide o_1 is already passed from an (i, j) location as shown in Fig. 4(a) or Fig. 4(b), then there is only one possible routing path for o_2 at (i, j) with the incoming from L and outgoing to RD. Similarly, the crossing constraints along the right-boundary grid points are shown in Figs. 4(c) and Fig. 4(d). The crossing constraints for the internal grid locations are presented in Figs. 4(e–r). When the previously routed waveguide (o_1) is present, as shown in Figs. 4(e) and (f), then o_2 can cross (i, j) in two possible ways, i.e., from L to (U or R) or from R to (U or L). To satisfy the physical design rule, o_2 cannot route to RD. However, in Fig. 4(g), o_2 can route in three different ways as represented. Similarly, all the cases are defined as depicted in Figs. 4(h–r).

Further, the implementation of *MBL* is explained in **Algorithm 1** that has *toplist*, *bottomlist* and N as inputs. As mentioned in lines 2–4, an ILP model is formulated for t different grids with the size of $[N \times 1, N \times 2, \ldots, N \times N]$ using Equations (5) to (13). Then the minimized cost function is performed on all t routings to find the best routing results. Hence, the total time complexity for *MBL* is equal to $\mathcal{O}(tN^2) = \mathcal{O}(N^3)$. In the next section, a heuristic is proposed for optical channel routing.

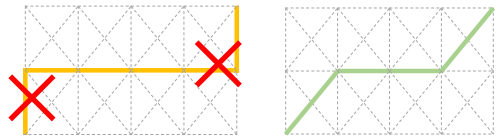

(a) (b)

Fig. 5: Optical waveguide bends during horizontal routing (a) without restriction and (b) with restriction.

5 Reducing Bend Loss (*RBL*) in Optical Channel Routing

The existing *TNR* algorithm show the horizontal movements of optical waveguides along tracks, which reduces the number of tracks as compared to *2SWAP*. Hence in this work, sharing of two optical waveguides along one track has been considered to reduce the tracks.

Further, the horizontal movement of optical waveguides in *TNR* routing have no restriction that results in a higher number of α (90°) bends and a few θ bends. The presence of these bends results in a higher bend loss due to sharp angles. Since the main objective of this work is to reduce the total bend loss, hence we have introduced a restricted routing of optical waveguides, as shown in Fig. 5. Fig. 5(a) shows the unrestricted horizontal routing, where an optical waveguide takes two α bends, resulting a bend loss of 0.738 dB. However, restricting the routing with a diagonal before and after the horizontal path reduces the total bend loss to 0.482 dB, as shown in Fig. 5(b). In this section, a heuristic for optical channel routing has been discussed that uses restricted movements.

A heuristic approach for the on-chip channel routing for reducing the bend loss (*RBL*) has been explained in **Algorithm 2**. The *RBL* is a grid-based channel routing algorithm, where all the waveguides are routed from bottom to top terminal list. The aim of this algorithm is to route all the waveguides from the bottom terminal list to the top terminals while reducing the total bend loss (*TBL*) and the number of tracks (T) inside the channel. As aforementioned, the *TBL* can be reduced by using the restricted horizontal routing, which replaces the smaller angles, i.e., α, θ angles

Algorithm 2 *RBL*

Input: *toplist*, *bottomlist*
Output: Routing results inside optical channel grid

6 *start* = 0; *end* = length(*bottomlist*); $T = 0$; *maxpos* = *minpos* = 0; **while** *all waveguides are not routed* **do**
7 *maxpos*, *minpos* = FindMaxMin(*bottomlist*, *start*, *end*); $R_{diff} = end - maxpos - 1$; $L_{diff} = minpos - start$; **if** $maxpos + 1 < minpos$ **then**
8 **if** $R_{diff} > L_{diff}$ **then**
9 RightMove(*bottomlist*, *maxpos*, *start*, *end*);
10 **else**
11 LeftMove(*bottomlist*, *minpos*, *start*, *end*);
12 **end**
13 **end**
14 **else**
15 LeftMove(*bottomlist*, *minpos*, *start*, *end*); RightMove(*bottomlist*, *maxpos*, *start*, *end*);
16 **end**
17 $T = T + 1$;
18 **end**

Algorithm 3 *RightMove*

Input: *bottomlist*, *maxpos*, *start*, *end*
Output: Routing results of the current track with the updated *bottomlist* inside optical channel grid

19 N = length(*bottomlist*); $r = end - maxpos - 2$;
20 **for** *all waveguides in bottomlist from (start, maxpos) and (end, N)* **do**
21 Move the waveguide in $U^{(1)}$ direction;
22 **end**
23 **if** $r \geq 0$ **then**
24 Route the *maxpos* waveguide in *bottomlist* by performing $RD^{(1)} \longrightarrow R^{(r)} \longrightarrow RD^{(1)}$;
25 **else**
26 Route the *maxpos* waveguide in *bottomlist* by performing $RD^{(1)} \longrightarrow U^{(1)}$;
27 **end**
28 **for** *all waveguides in bottomlist from (maxpos+1, end)* **do**
29 Move the waveguide in $LD^{(1)}$;
30 **end**
31 Decrement the *end* by 1; Update the *bottomlist* with this routed path; **return** *Routing results of current track with the updated bottomlist inside optical channel grid;*

with the larger angles, i.e., $\alpha + \theta$, $\alpha + \phi$, and 2θ angles.

Algorithm 2 describes the *RBL* algorithm that has two inputs *toplist* and *bottomlist*, where *toplist* and *bottomlist* are the terminal list of top and bottom boundaries of the optical channel. The four data variables *start*, *end*, *minpos*, and *maxpos* are used in *RBL*, where *start* and *end* variables point to the start and end locations of the unrouted terminal list in the current track; however, *minpos* and *maxpos* point to those locations of the unrouted waveguide that have minimum and maximum terminal numbers, respectively in the current track. Initially, no waveguide is routed; hence *start* and *end* are initialized with first and last indices of *bottomlist* (line 1). The *maxpos* and *minpos* are initiated to 0 (line 1), which are further updated with the FindMaxMin function (line 3) that returns the *maxpos* and *minpos* from the terminal list in the range of *start* and *end*. On each track, waveguides are routed by performing one or two horizontal left or right moves. The waveguide movement depends on the *maxpos* and *minpos* on the current track, which is described in **Algorithm 2** with the following cases: **case (i)** routes *maxpos* waveguide at the *end* location by performing a RightMove (line 7-8), which has been explained in **Algorithm 3**, **case (ii)** routes *minpos* waveguide at the *start* location by performing a LeftMove (line 10), and **case (iii)** shows the sharing of tracks by two waveguides while performing both right and LeftMove (line 14-15).

The horizontal routing in all three cases follows the restricted routing by replacing the $U \rightarrow L/R \rightarrow U$ moves with $RD \rightarrow R \rightarrow RD$ and $LD \rightarrow L \rightarrow LD$ for right and left routing, respectively (as depicted in Fig. 5). When *minpos* becomes higher than the $maxpos + 1$, then the horizontal path for the waveguides at *minpos* and *maxpos* overlaps with each other (line 6-11). Hence, **case (i)** and **(ii)** route a single waveguide in horizontal right or left direction from *maxpos* or *minpos*, respectively (line 7-10). However, when the *minpos* location is smaller as compared to $maxpos + 1$, then the same track can be simultaneously used by two waveguides

for both right and left moves (line 13-16). The selection of **case (i)** or **case (ii)** depends on R_{diff} and L_{diff}, where R_{diff} and L_{diff} are the difference of *maxpos* and *minpos* from the *end* and *start*, respectively. When R_{diff} is more than L_{diff}, then RightMove is performed on waveguide at *maxpos* (line 8). Otherwise, LeftMove is performed on waveguide at *minpos* (line 10). Further, the complete routing for these three cases has been outlined in detail in **Algorithm 3**.

1) RightMove: The RightMove of *RBL* has been explained in **Algorithm 3**, that takes the current track *bottomlist*, *maxpos*, *start*, and *end* as its input. In addition to the horizontal right routing, this algorithm also updates the locations of the remaining waveguides. All the waveguides on the left-side of *maxpos* and on the right-side of *end* are moved in one vertical up direction, i.e., $U^{(1)}$ (line 3-4). The horizontal restricted routing has been detailed in line 6-11, where r denotes the number of steps to be taken by waveguide at *maxpos* in the right direction. When $r \geq 0$, then the *maxpos* waveguide routes by taking one-step right-diagonal ($RD^{(1)}$), r-step right ($R^{(r)}$), and one-step right-diagonal ($RD^{(1)}$), which has been presented as $RD^{(1)} \longrightarrow R^{(r)} \longrightarrow RD^{(1)}$. However, when *maxpos* is immediately left to the *end* location then waveguide does not require any horizontal move. Hence the waveguide route by taking one-step right-diagonal ($RD^{(1)}$) and then one-step vertical up ($U^{(1)}$) moves, that is represented as $RD^{(1)} \longrightarrow U^{(1)}$. The remaining waveguides positioned in between $(max + 1, end)$ move one-step left-diagonal, i.e., $LD^{(1)}$ (line 12-13). At the end, *end*, T, and *bottomlist* are updated (line 15-17).

2) LeftMove: Similar to the RightMove, a restricted horizontal left routing at *minpos* has been implemented. In the LeftMove algorithm, waveguides replace the RD and R moves of **Algorithm 3** with LD and L directional moves.

In **Algorithm 2**, *maxpos* and *minpos* are found in $\mathcal{O}(N)$ and then routing of all the waveguides on current track is performed with RightMove or LeftMove in $\mathcal{O}(N)$. $\mathcal{O}(N) + \mathcal{O}(N)$ operations are performed until all the waveguides are routed, i.e., for T times. Hence, the total time complexity for *RBL* is equal to $\mathcal{O}(NT)$.

6 Simulation Results and Discussion

This section presents the simulation results with the comparative analysis of the proposed algorithms.

6.1 Simulation Results

In this section, the proposed *MBL* and *RBL* are compared with the existing *2SWAP* [13], and *TNR* [14] algorithms in terms of signal loss and area used. All the algorithms are implemented in Python 3.7.4 and run on Intel Core i7-9750H CPU 2.60GHz machine with 8 GB memory. In order to perform the comparative analysis, different testcases are randomly generated with a varying number of terminals (N).

An illustration of optical channel routing implementation for the prior works (*2SWAP* [13] and *TNR* [14]) and the proposed algorithms (*MBL*, *RBL*) is presented with an example in Fig. 6, which provides a better understanding of bending effects while routing. As the smaller bend radius introduces the excess loss and crosstalk between different waveguides and the larger bending radii occupy a larger footprint. Hence, the minimum and maximum bend radius are satisfied by considering w and h as 1 and 1.732 units, respectively, resulting in $\alpha = 90°$, $\theta = 60°$, $\alpha+\theta = 150°$, $\alpha + \phi = 120°$, $2\theta = 120°$ angles [14, 21]. The $BL(\theta)$, $BL(\alpha)$, $BL(\alpha + \phi)$, $BL(\alpha + \theta)$, and $BL(2\theta)$ are 0.592, 0.369, 0.204, 0.204 and 0.074 (dB), respectively (from Equation (1)). Fig. 6(a) shows the optical channel routing for the *2SWAP*, which takes a total of 20 bends with a bend angle of $\alpha+\theta$ and a total number of 6 tracks (T). Hence, *TBL* for *2SWAP* is 1.5 dB. The routing result of *TNR* has been represented in Fig. 6(b), which uses a total of 6, 7 and 3 number of α, $\alpha + \theta$, and 2θ bends. Hence *TBL* for *TNR* is 3.4 dB, which is higher as compared to *2SWAP*. This increase in *TBL* is due to the presence of smaller bends (α) in *TNR*. However, T in *TNR* is reduced to 4, resulting in a smaller channel area than *2SWAP*. Similarly, the calculated *TBL* for *MBL*, and *RBL* algorithms are 1.3, and 2.3 dB, respectively. The absence of α and θ bends in *RBL* results in the

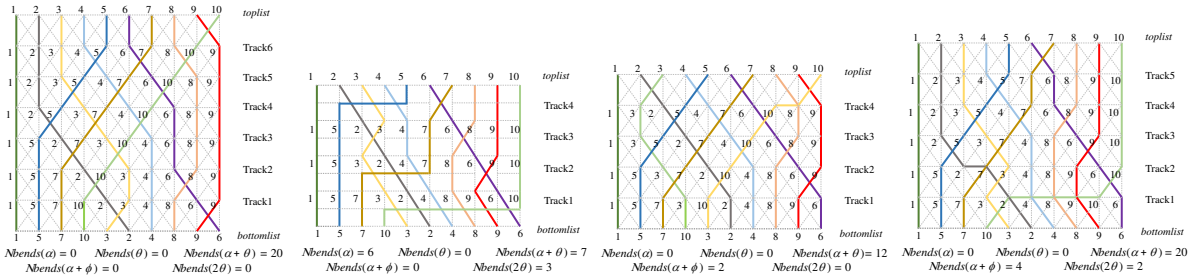

(a) (b) (c) (d)

Fig. 6: An example of channel routing using (a) *2SWAP* [13], (b) *TNR* [14], (c) *MBL*, and (d) *RBL*.

Table 2: Comparative result of the proposed *MBL* and *RBL* algorithms with the previous algorithms in terms of number of bendings, where $Nbends(x)$ represent the total number of bends with x-angle for different testcases varying with the number of terminals (N) for an optical channel.

testcase	N	Previous Algorithms		Proposed		
		***2SWAP* [13]**	***TNR* [14]**	***MBL***		***RBL***
		$Nbends(\alpha+\theta)$	$Nbends(\alpha)$, $Nbends(\alpha+\theta)$, $Nbends(2\theta)$	$Nbends(\alpha), Nbends(\theta)$, $Nbends(\alpha+\phi)$, $Nbends(\alpha+\theta), Nbends(2\theta)$	**Time (hrs)**	$Nbends(\alpha+\phi)$, $Nbends(\alpha+\theta)$, $Nbends(2\theta)$
TC–1	10	12	4, 6, 2	0, 0, 0,12, 0	2.6	4, 24, 0
TC–2	15	24	12, 6, 3	0, 0, 20, 0, 0	5.3	8, 19, 1
TC–3	20	50	18, 25, 3	0, 0, 2, 43, 0	12.1	14, 40, 8
TC–4	25	54	20, 25, 3	0, 0, 2, 47, 0	15.2	14, 43, 10
TC–5	30	92	28, 37, 7	0, 0, 8, 47, 2	17.8	22, 52, 17
TC–6	50	256	166, 200, 191	—	—	301, 78, 170
TC–7	70	588	370, 395, 389	—	—	114, 695, 362
TC–8	80	668	442, 458, 407	—	—	136, 769, 379
TC–9	90	760	554, 520, 397	—	—	160, 1086, 558
TC–10	100	1116	652, 845, 784	—	—	160, 1360, 509

reduction of *TBL* with an overhead of an increased T compared to *TNR*, as shown in Fig. 6(d). Further, this overhead is removed in *MBL*, which has both the least number of tracks ($T = 4$) and *TBL* (1.3 dB), as depicted in Fig. 6(c).

As shown in Tables 2, 3, and 4, ten testcases (TC–1 to TC–10) with $N = (10, 15, \ldots, 100)$ are randomly generated that have two terminal lists named as *toplist* and *bottomlist* along the top and bottom boundaries of the optical channel, respectively. Both lists are initialized with a different integer number in the range of $[1, n]$. In Table 2, $Nbends(x)$ denote the total number of bends with x-angle. The proposed *MBL* is simulated and compared for $N \leq 30$ due to the high execution time. Hence a '—' in Tables 2, 3, and 4 indicate that the testcase is not being run for the respective N value. In Table 3, *TBL* is the total bend loss in dB, *TPL* is the total propagation loss in 10^{-6} units, *TCL* is the total crossing loss, and *WSL* is the worst signal loss in dB. In Table 4, T denotes the number of tracks, and *TWL* is the total waveguide length in the optical channel grid. A comparative study of the proposed *MBL* and *RBL* with the previous algorithms is shown in Tables 2, 3, and 4.

Since the objective of our work is to minimize the signal loss while reducing the area. Hence, the comparative results in Table 3 show that the proposed *MBL* outperforms in terms of signal loss as compared to the previous algorithms and the proposed *RBL* while maintaining a better balance for tracks compared to *2SWAP* and *RBL* (as shown in Table 4). Tables 3 and 4 show that the *MBL* has an average reduction of 57.9% and 63.1% in *TBL* and *WSL*, respectively, with an increase of 12.7% and 9.8% in T and *TWL*, respectively, compared to *TNR*. However, compared to *2SWAP*, *MBL* shows an average reduction of 44.8%, 38.1%, 25.4%, 5.8%

Table 3: Comparative result of the proposed *MBL* and *RBL* algorithms with the previous algorithms in terms of signal loss, i.e., total bend loss (*TBL*), total propagation loss (*TPL*) in 10^{-6} units, total crossing loss (*TCL*), and worst signal loss (*WSL*) ↓ and ↑ indicate the reduction and increment percentage, respectively.

testcase	⟨ *TBL*, *TPL*, *TCL*, *WSL* ⟩							
	Previous Algorithms		**Proposed**	***MBL*% change w.r.t. [13]**	***MBL*% change w.r.t. [14]**	**Proposed**	***RBL* % change w.r.t. [13]**	***RBL* % change w.r.t. [14]**
	***2SWAP* [13]**	***TNR* [14]**	***MBL***	⟨ ↓, ↑, ↓, ↓⟩	⟨ ↓, ↑, ↓, ↓⟩	***RBL***	⟨ ↑, ↑, ↓, ↑⟩	⟨ ↓, ↑, ↓, ↓⟩
TC–1	⟨ 1.6, 0.1, 2, 0.41 ⟩	⟨ 2.3, 0.15, 2, 0.8 ⟩	⟨ 0.8, 0.3, 2, 0.22 ⟩	⟨ 50, 66.7, 0, 46.3 ⟩	⟨ 65.2, 50, 0, 72.5 ⟩	⟨ 2.6, 0.34, 2, 0.7 ⟩	⟨ 38.5, 70.6, 0, 41.4 ⟩	⟨−13.1, 55.9, 0, 12.5 ⟩
TC–2	⟨ 3.24, 0.2, 2.6, 0.8 ⟩	⟨ 5.3, 0.2, 2.6, 1.4 ⟩	⟨ 1.8, 0.3, 2.6, 0.44 ⟩	⟨ 44.4, 33.3 0, 45 ⟩	⟨ 66.1, 33.3, 0 68.6 ⟩	⟨ 3.2, 0.3, 2.6, 0.8 ⟩	⟨−1.25, 33.3 0, 0 ⟩	⟨ 39.6, 33.3, 0, 42.9 ⟩
TC–3	⟨ 6.7, 0.5, 7.8, 1.2 ⟩	⟨ 9.1, 0.5, 7.8, 2.1 ⟩	⟨ 3.5, 0.6 7.8, 1.1 ⟩	⟨ 47.8, 16.7, 0, 8.33 ⟩	⟨ 61.6, 16.7, 0, 47.7 ⟩	⟨ 7.4, 1.2, 7.8, 1.8 ⟩	⟨ 9.5, 58.3, 0, 33.3 ⟩	⟨ 18.7, 58.3, 0, 14.3 ⟩
TC–4	⟨ 7.3, 0.6, 8.4, 1.4 ⟩	⟨ 9.7, 0.5, 8.4, 2.3 ⟩	⟨ 4.2, 0.7, 8.4, 0.8 ⟩	⟨ 42.7, 25.7, 0, 42.9 ⟩	⟨ 56.7, 32.2, 0, 65.2 ⟩	⟨ 8.1, 0.6, 8.4, 1.4 ⟩	⟨ 9.9, 0, 0, 0 ⟩	⟨ 16.5, 8.7, 0, 39.1 ⟩
TC–5	⟨ 12.4, 0.9, 16.2, 2.1 ⟩	⟨ 14.5, 0.7, 16.2, 3.3 ⟩	⟨ 6.9, 0.9, 16.2, 1.1 ⟩	⟨ 44.4, 0, 0, 47.6 ⟩	⟨ 52.4, 22.2, 0, 66.7 ⟩	⟨ 11.8, 0.9, 16.2, 1.8 ⟩	⟨−5.1, 22, 0, − 16.7 ⟩	⟨ 18.6, 23.9, 0, 45.5 ⟩
TC–6	⟨ 34.6, 8.2, 143.6, 1.5 ⟩	⟨ 115.23, 9.23, 143.6, 5.1 ⟩	—	—	—	⟨ 73.2, 8.5, 143.6, 2.8 ⟩	⟨ 52.7, 3.8, 0, 46.4 ⟩	⟨ 36.5, −8.2, 0, 45.1 ⟩
TC–7	⟨ 79.4, 17.6, 263.4, 2.7 ⟩	⟨ 245.54, 16.9, 263.4, 7.9 ⟩	—	—	—	⟨ 149.2, 17.7, 263.4, 4.7 ⟩	⟨ 46.8, 0.8, 0, 42.6 ⟩	⟨ 39.2, 4.8, 0, 40.5 ⟩
TC–8	⟨ 92.9, 21.1, 325.2, 2.9 ⟩	⟨ 280.5, 22.2, 325.2, 7.3 ⟩	—	—	—	⟨ 162.7, 21.4, 325.2, 4.2 ⟩	⟨ 42.9, 1.4, 0, 30.9 ⟩	⟨ 41.9, −3.7, 0, 42.5 ⟩
TC–9	⟨ 102.7, 27.2, 425.6, 2.3 ⟩	⟨ 320.3, 25.9, 425.6, 10.1 ⟩	—	—	—	⟨ 227.9, 27.6, 425.6, 5.4 ⟩	⟨ 54.9, 1.4, 0, 57.4 ⟩	⟨ 28.8, 6.2, 0, 46.5 ⟩
TC–10	⟨ 150.77, 35.8, 489.4, 3.7 ⟩	⟨ 463.9, 33.2, 489.4, 10.3 ⟩	—	—	—	⟨ 238.4, 33.3, 489.4, 6.1 ⟩	⟨ 36.8, −7.4, 0, 39.3 ⟩	⟨ 48.6, 0.39, 0, 40.8 ⟩
Average				⟨ 44.8, 20.8, 0, 38.1 ⟩	⟨ 57.9, 27.7, 0, 63.1 ⟩	**Average**	⟨ 44.4, −0.2, 0, 35.9 ⟩	⟨ 39.7, 2.2, 0, 41.3 ⟩

Table 4: Comparative result of the proposed *MBL* and *RBL* algorithms with the previous algorithms in terms of area, i.e., Tracks (*T*), and total wire length (*TWL*) ↓ and ↑ indicate the reduction and increment percentage, respectively.

testcase	⟨*T*, *TWL*⟩							
	Previous Algorithms		**Proposed**	***MBL*% change w.r.t. [13]**	***MBL*% change w.r.t. [14]**	**Proposed**	***RBL*% change w.r.t. [13]**	***RBL*% change w.r.t. [14]**
	***2SWAP* [13]**	***TNR* [14]**	***MBL***	⟨ ↓, ↑⟩	⟨ ↑, ↑⟩	***RBL***	⟨ ↓, ↑⟩	⟨ ↑, ↑⟩
TC–1	⟨4, 58.3⟩	⟨3, 48.9⟩	⟨4, 60.3⟩	⟨0, 3.3⟩	⟨25, 18.9⟩	⟨6, 115.4⟩	⟨−50, 49.5⟩	⟨50, 57.6⟩
TC–2	⟨ 8, 67.2⟩	⟨ 5, 70.1⟩	⟨ 6, 71.3⟩	⟨ 25, 5.8⟩	⟨ 16.7, 1.7 ⟩	⟨ 7, 128.1⟩	⟨12.5, 47.5⟩	⟨28.6, 45.3⟩
TC–3	⟨ 13, 182.3⟩	⟨ 9, 167.4⟩	⟨ 11, 184.2⟩	⟨ 15.4, 1.1⟩	⟨ 18, 9.1⟩	⟨ 12, 240.6⟩	⟨7.6, 24.2⟩	⟨25, 30.4⟩
TC–4	⟨ 15, 203.3⟩	⟨ 11, 167.4⟩	⟨ 12, 199.1⟩	⟨ 20, − 2.1⟩	⟨ 8.3, 15.9⟩	⟨ 13, 254⟩	⟨13.3, 19.9⟩	⟨15.4, 34.1⟩
TC–5	⟨23, 310.5⟩	⟨13, 244.2⟩	⟨14, 259.1⟩	⟨39.1, − 19.8⟩	⟨7.1, 5.7⟩	⟨16, 321.9⟩	⟨30.4, 3.5⟩	⟨18.8, 24.1⟩
TC–6	⟨42, 2744.8⟩	⟨28, 3075.5⟩	—	—	—	⟨33, 2856.9⟩	⟨21.5, 3.9⟩	⟨15.2, − 7.7⟩
TC–7	⟨67, 5851.1⟩	⟨36, 5626.9⟩	—	—	—	⟨48, 5901.2⟩	⟨28.4, 0.8⟩	⟨25, 4.6⟩
TC–8	⟨70, 7027.1⟩	⟨43, 7410.4⟩	—	—	—	⟨56, 7125.9⟩	⟨20, 1.4⟩	⟨23.21, − 4.1⟩
TC–9	⟨80, 9052.9⟩	⟨46, 8642.4⟩	—	—	—	⟨61, 8923.1⟩	⟨23.8, − 1.4⟩	⟨24.6, 3.1⟩
TC–10	⟨98, 11927.2⟩	⟨48, 11058.6⟩	—	—	—	⟨65, 11100.4⟩	⟨33.7, − 7.5⟩	⟨26.1, 0.4⟩
Average				⟨25.4, −6.1⟩	⟨12.7, 9.8⟩	**Average**	⟨24.5, −1.3⟩	⟨23.7, 1.2⟩

in *TBL*, *WSL*, *T*, and *TWL*, respectively. Further, in comparison to *RBL*, *MBL* shows an average reduction of 48.1%, 43.7%, 12.9%, 26.9% in *TBL*, *WSL*, *T*, and *TWL*, respectively for first five testcases (TC-1 to TC–5). Hence, these results show that the proposed *MBL* outperforms the prior works and the proposed *RBL* in terms of signal loss. However, *MBL* faces the scalability issue when the input size is increased. Therefore, we proposed a heuristic *RBL* which resolves this issue.

In Table 3, the simulation results show *2SWAP* algorithm shows the least *TBL* as compared to *TNR* and the proposed *RBL*. However, it has a cost of higher *T*, as compared in Table 4. Hence *2SWAP* requires a larger chip area to implement. In Table 2, the simulation results show *RBL* does not have α and θ bends, which is due to the restricted horizontal routing that eliminated the smaller bend angles. This elimination of smaller bends helps to reduce the *TBL* in *RBL* compared

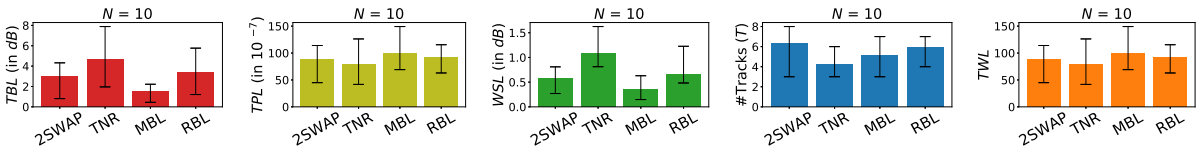

(a) (b) (c) (d) (e)

Fig. 7: Average comparative results of proposed and previous algorithms in terms of (a) total bend loss (TBL), (b) total propagation loss (TPL), (c) worst signal loss (WSL), (d) number of tracks (T), and (e) total waveguide length (TWL) over 30 different testcases having $N = 10$.

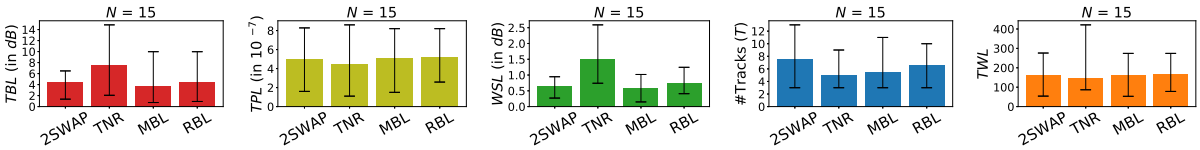

(a) (b) (c) (d) (e)

Fig. 8: Average comparative results of proposed and previous algorithms in terms of (a) total bend loss (TBL), (b) total propagation loss (TPL), (c) worst signal loss (WSL), (d) number of tracks (T), and (e) total waveguide length (TWL) over 30 different testcases having $N = 15$.

to *TNR*. In terms of T, *TNR* uses the least tracks at the cost of higher *TBL* and *WSL*, which results in the reduced signal strength at the output. The proposed *RBL* algorithm provides balanced results between *2SWAP* and *TNR* while reducing *TBL*, *WSL*, *TWL* and T. In *RBL*, all the testcases except TC–1 (red text in Table 3) show the reduction of *TBL*, *WSL* and T in comparison to *TNR*. This is due to the higher number of bendings in *RBL* and fewer α bends in *TNR* for the smaller input terminals. Hence, the proposed *RBL* algorithm shows a better reduction in all the routing parameters for the larger testcases having $N > 10$. The comparative results show that the proposed *RBL* has an average reduction of 24.5%, 1.2% and 0.21% in T and *TWL*, and *TPL*, respectively, with an increase of 44.4% and 35.9% in *TBL* and *WSL*, respectively, compared to *2SWAP*. This increase in TBL and WSL is due to the increasing number of bendings in *RBL*, as shown in Table 2. However, in comparison to *TNR*, the proposed *RBL* has an average reduction of 39.7%, 2.2%, and 41.3%, and in *TBL*, *TPL*, and *WSL*, respectively, with an increase of 23.7% and 1.2% in T and *TWL*, respectively. Therefore, these results conclude that the increase in T reduces the bends, which results in the reduction of signal loss with an overhead of increased area.

Further, Figs. 7 and. 8 show the average comparative results of 30 different testcases having $N = 10$ and 15, respectively. The total execution time for the average analysis is 78 and 248 hours for $N = 10$ and 15, respectively. Since, the execution time for $N > 15$ is high, therefore we have considered an average comparative analysis for the 30 different testcases for $N = 10$ and 15 only. Figs. 7(a and c) and 8(a and c) show that *MBL* has the least *TBL* and *WSL* compared to *2SWAP*, *TNR*, and *RBL*, which is due ato the minimization of smaller bends and total number of bends. This minimization of bend and worst signal losses shows the increment in T compared to the optimal method, i.e., *TNR* (Figs. 7(d) and 8(d)), which further increases the *TWL* (Figs. 7(e) and 8(e)) and *TPL* (Figs. 7(b) and 8(b)). Hence, these results show that there is a trade-off in between the minimization of loss and area. However, in comparison to the proposed *RBL*, the *MBL* shows the reduction in both loss and area. Hence, the simulation results conclude that for some smaller testcases with $N \leq 10$, the *RBL* does not perform well in terms of both optical losses and T, hence for such cases, *MBL* is preferred over *RBL*.

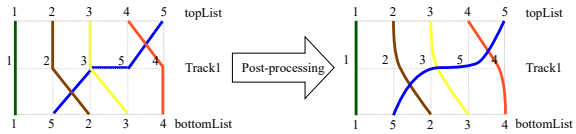

Fig. 9: An example of post-processing in *MBL* and *RBL*.

However, for the large testcases when time is the constraint, then *RBL* can be chosen over *MBL*.

6.2 Discussion

The gridless optical routing in [6] presented a list of routing geometries where the optical waveguides are bend curvily. In the proposed grid-based channel routing, the optical waveguide curvilinear nature can be satisfied in the post-processing step, as shown in Fig. 9.

7 Conclusions

In this paper at first, we propose an ILP formulation for minimizing the bend loss (*MBL*) in the optical channel routing for photonic integrated circuits. The proposed *MBL* results in the minimization of total bend loss and worst signal loss while reducing the number of tracks in comparison to the state-of-art techniques. However, the execution time of *MBL* is very high for larger testcases. Hence a scalable heuristic for reducing the bend loss (*RBL*) is proposed. The proposed *RBL* algorithm eliminates the smaller bending which shows a balanced result between the bend loss and track reduction, as compared to the state-of-the-art techniques. *RBL* reduces the bend loss with an overhead of increased number of tracks, which, in turn, increases the waveguide length and the channel area.

Acknowledgments. This work by S. Sharma was supported by the Ministry of Electronics and Information Technology (MeitY), Govt. of India (grant #: MEITY-1100-CSE). This work by S. Roy was supported by the FIG research grant of the Indian Institute of Technology Roorkee sponsored by the MHRD, Govt. of India.

Declarations

Conflict of interest. The authors declare that they have no confict of interests.

References

[1] M. Smit, J. Tol, M. Hill, Moore's Law in Photonics. Wiley Laser & Photonics Reviews **6**(1), 1–13 (2012)

[2] S. Sharma, S. Roy, A Survey on Design and Synthesis Techniques for Photonic Integrated Circuits. Springer Journal of Supercomputing **77**(5), 4332–4374 (2021)

[3] K. Kitayama, M. Notomi, M. Naruse, et al., Novel Frontier of Photonics for data Processing–Photonic Accelerator. APL Photonics **4**(090901), 1–24 (2019)

[4] S. Werner, J. Navaridas, et al., A Survey on Optical Network-on-Chip Architectures. ACM Computing Survey **50**(6), 1–37 (2018)

[5] J. Bashir, E. Peter, et al., A Survey of On-Chip Optical Interconnects. ACM Computing Survey **51**(6), 1–34 (2019)

[6] D. Ding, Y. Zhang, H. Huang, et al., in *Proc. of the ACM/IEEE Design Automation Conference (DAC)* (2009), pp. 264–269

[7] Y.K. Chuang, K.J. Chen, K.L. Lin, et al., in *Proc. of the ACM/IEEE Design Automation Conference (DAC)* (2018), pp. 151:1–151:6

[8] A. Truppel, T.M. Tseng, et al., PSION+: Combining Logical Topology and Physical Layout Optimization for Wavelength-Routed ONoCs. IEEE Transactions on Computer-Aided Design of Integrated Circuits and Systems) **26**(12), 5197–5197 (2020)

[9] Z. Zheng, M. Li, et al., in *Proc. of the Asia and South Pacific Design Automation Conference (ASPDAC)* (2021), pp. 568–573

[10] A.V. Beuningen, L. Ramini, D. Bertozzi, et al., PROTON+: A Placement and Routing Tool for 3D Optical Networks-on-Chip with a Single Optical Layer. ACM Journal of Emerging Technologies in Computing Systems **12**(4), 44:1–44:28 (2015)

[11] D. Liu, Z. Zhao, Z. Wang, et al., in *Proc. of the ACM/IEEE Design Automation Conference (DAC)* (2018), pp. 1–6

[12] C. Condrat, P. Kalla, S. Blair, in *Proc. of the ACM/IEEE International Workshop on System Level Interconnect Prediction (SLIP)* (2013), pp. 1–8

[13] C. Condrat, P. Kalla, S. Blair, Crossing-Aware Channel Routing for Integrated Optics. IEEE Transactions on Computer-Aided Design of Integrated Circuits and Systems **33**(6), 814–825 (2014)

[14] J. Yan, On-Chip Optical Channel Routing for Signal Loss Minimization. IEEE Transactions on Computer-Aided Design of Integrated Circuits and Systems **37**(8), 1654–1666 (2018)

[15] C. Condrat, P. Kalla, S. Blair, in *Proc. of the IEEE International Midwest Symposium on Circuits and Systems (MWSCAS)* (2012), pp. 598–601

[16] K. Chaudhary, P. Robinson, Channel Routing by Sorting. IEEE Transactions on Computer-Aided Design of Integrated Circuits and Systems **10**(6), 754–760 (1991)

[17] J. Yan, An Improved Optimal Algorithm for Bubble-sorting-based Non-Manhattan Channel Routing. IEEE Transactions on Computer-Aided Design of Integrated Circuits and Systems **38**(2), 163–171 (1999)

[18] S. Jahani, S. Kim, et al., Controlling Evanescent Waves using Silicon Photonic All-dielectric Metamaterials for Dense Integration. Nature Communications **9**(1893), 1–9 (2018)

[19] Z. Li, G. Li, et al., Ultra-compact High Efficiency and Low Crosstalk Optical Interconnection Structures based on Inverse Designed Nanophotonic Elements. Scientific Reports **10**(11993) (2020)

[20] W. Bogaerts, L. Chrostowski, Silicon Photonics Circuit Design: Methods, Tools and Challenges. Wiley Laser & Photonics Reviews **12**(4), 1700,237:1–1700,237:29 (2018)

[21] S. Sharma, S. Roy, in *Proc. of the International Conference on VLSI Design and International Conference on Embedded Systems (VLSID)* (2021), pp. 246–251